LETTERS

The depolymerizing kinesin MCAK uses lattice diffusion to rapidly target microtubule ends

Jonne Helenius[1]*, Gary Brouhard[1]*, Yannis Kalaidzidis[1,2], Stefan Diez[1] & Jonathon Howard[1]

The microtubule cytoskeleton is a dynamic structure in which the lengths of the microtubules are tightly regulated. One regulatory mechanism is the depolymerization of microtubules by motor proteins in the kinesin-13 family[1]. These proteins are crucial for the control of microtubule length in cell division[2–4], neuronal development[5] and interphase microtubule dynamics[6,7]. The mechanism by which kinesin-13 proteins depolymerize microtubules is poorly understood. A central question is how these proteins target to microtubule ends at rates exceeding those of standard enzyme–substrate kinetics[8]. To address this question we developed a single-molecule microscopy assay for MCAK, the founding member of the kinesin-13 family[9]. Here we show that MCAK moves along the microtubule lattice in a one-dimensional (1D) random walk. MCAK–microtubule interactions were transient: the average MCAK molecule diffused for 0.83 s with a diffusion coefficient of 0.38 $\mu m^2 s^{-1}$. Although the catalytic depolymerization by MCAK requires the hydrolysis of ATP, we found that the diffusion did not. The transient transition from three-dimensional diffusion to 1D diffusion corresponds to a "reduction in dimensionality"[10] that has been proposed as the search strategy by which DNA enzymes find specific binding sites[11]. We show that MCAK uses this strategy to target to both microtubule ends more rapidly than direct binding from solution.

Kinesin-13 motor proteins act at microtubule ends, where they are thought to force protofilaments into a curved conformation[12,13], which is a likely structural intermediate in the depolymerization process[14]. Classically, kinesin motor proteins reach microtubule ends by ATP-dependent translocation along microtubules. However,

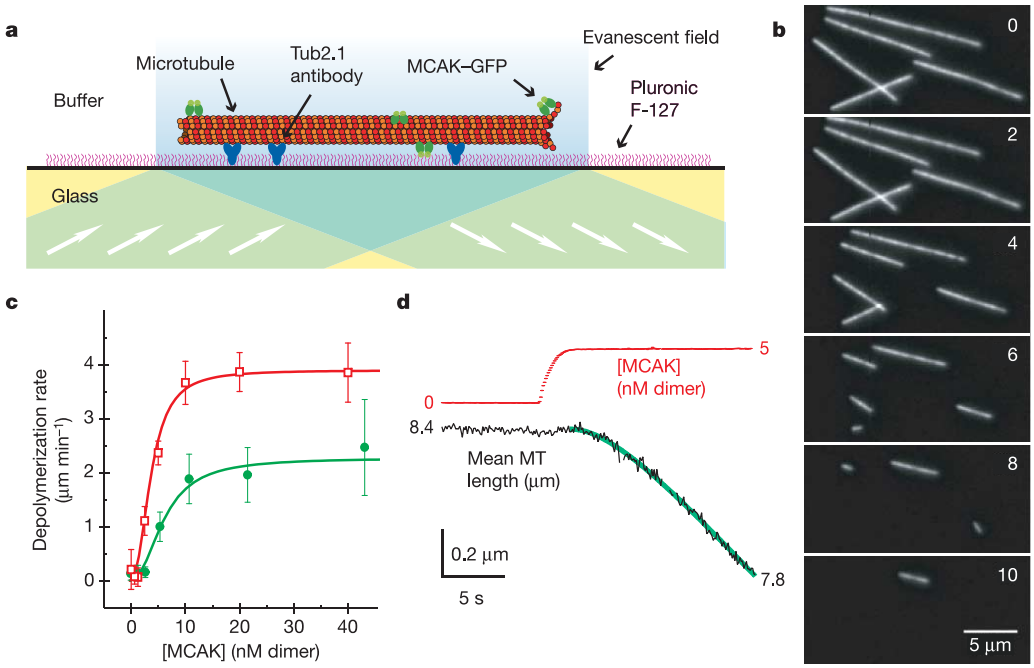

Figure 1 | MCAK-dependent microtubule depolymerization. a, Diagram of the *in vitro* assay depicting a microtubule (red) immobilized above the glass surface by anti-tubulin antibodies (dark blue). Excitation by total internal reflection allows the detection of single molecules (namely MCAK–GFP in green) in the evanescent field (shown in blue). **b**, Epifluorescence images of immobilized microtubules at the times shown in minutes. MCAK dimer (8 nM) was added at $t = 2$ min. **c**, Plot of microtubule depolymerization rate against MCAK concentration. Error bars are s.d. Data fitted to Hill equations (lines plotted) yielded $K_m = 3.9$ nM and $K_m = 6.1$ nM for MCAK and MCAK–GFP, and $n = 2.4$ and $n = 2.2$, respectively. Red squares, MCAK–His_6; green circles, MCAK–His_6–EGFP. **d**, Shortening of four microtubules from a mean length of 8.4 mm to 7.8 mm (black line) after the addition of 5 nM MCAK (red line). The depolymerization rate approached steady state with a time constant of 3.8 s (green fitted line).

[1]Max Planck Institute of Molecular Cell Biology and Genetics, Dresden 01307, Germany. [2]A. N. Belozersky Institute of Physico-Chemical Biology, Moscow State University, Moscow 119899, Russia.
*These authors contributed equally to this work.

directed motion has not been shown for kinesin-13 members[8]. To address the question of how kinesin-13 proteins reach microtubule ends, we expressed and purified two functional full-length versions of human MCAK: MCAK and green fluorescent protein (GFP)-tagged MCAK. We then developed a single-molecule microscopy assay for depolymerization (Fig. 1a) in which microtubules were immobilized on coverslips by means of surface-adsorbed anti-tubulin antibodies. Individual rhodamine-labelled microtubules and single MCAK–GFP molecules were revealed by epifluorescence and total-internal-reflection fluorescence (TIRF) illumination, respectively.

MCAK rapidly depolymerized GMP-CPP-stabilized microtubules in the depolymerization assay (Fig. 1b, and Supplementary movie 1). GMP-CPP (a slowly hydrolysable GTP analogue) was used to mimic the GTP found in the endcap of growing microtubules[15]. Depolymerization was ATP dependent and occurred at both microtubule ends. The depolymerization rate increased from its basal rate of $0.02\,\mu m\,min^{-1}$ to a peak rate of $3.9\,\mu m\,min^{-1}$ at 10 nM MCAK dimer (Fig. 1c). Thus, MCAK accelerated depolymerization up to 200-fold, with the maximum rate corresponding to about 50 tubulin dimers removed per second per microtubule end.

MCAK reached the microtubule ends very quickly. Microtubule lengths were measured after rapid infusion of MCAK into the observation chamber (Fig. 1d). On addition of 5 nM MCAK dimer, the depolymerization rate approached steady state with a rate constant, k, of $0.26\,s^{-1}$. This rate constant is related to the association rate to protofilament ends ($k_a = k[M]^{-1}$ when the MCAK concentration, [M], is much greater than the Michaelis constant, K_m), and k_a must therefore be on the order of $50\,\mu M^{-1}\,s^{-1}$. Five experiments at either 5 or 10 nM MCAK gave an on-rate of $51 \pm 12\,\mu M^{-1}\,s^{-1}$ (results are means ± s.e.m. unless otherwise indicated). This confirms previous stopped-flow experiments[8]. Given that each microtubule has 14 protofilaments, we infer an association rate of about $700\,\mu M^{-1}\,s^{-1}$ to empty microtubule ends. These rates are significantly higher than expected for protein–protein association by three-dimensional diffusion in solution[16]; for example, the association of tubulin dimers onto the ends of growing microtubules occurs with an association rate of $2–5\,\mu M^{-1}\,s^{-1}$ (refs 16, 17).

These kinetic data suggest that the targeting of MCAK to the microtubule ends is somehow facilitated. To investigate this we performed experiments at MCAK–GFP concentrations that allowed single molecules to be observed (see Supplementary Information 1 for an analysis showing that single MCAK–GFP dimers were observed). Unlike other kinesins, which undergo directed movement on the microtubule lattice, we found that single MCAK–GFP molecules performed a random walk on the lattice during their transient interaction with a microtubule (Fig. 2a, and Supplementary movie 2). Using an in-house software package[18], we tracked 1,147 MCAK–microtubule interactions that lasted longer than 0.4 s and calculated the diffusion coefficient, D, of MCAK–GFP to be $0.38 \pm 0.01\,\mu m^2\,s^{-1}$ (Fig. 2b, Methods, and Supplementary Information 1). The interaction times were distributed exponentially (Fig. 2c), with a mean lifetime, $\langle t \rangle$, of 0.83 ± 0.05 s when corrected for photobleaching (Supplementary Information 1). At no time did we observe a directional bias in the diffusion (Supplementary Information 1).

The diffusion coefficient is high. Viewing diffusion as a random walk, the diffusion coefficient is related to the step size (δ) and the time per step (τ) by $D = \delta^2/2\tau$ (ref. 17). If $\delta = 8$ nm (corresponding to stepping between tubulin dimers along a protofilament), then $\tau = 0.084$ ms, implying that MCAK takes 12,000 diffusive steps per second. This is more than 100-fold faster than kinesin-1 steps directionally along the microtubule lattice[19].

To what extent does 1D diffusion increase the rate at which MCAK finds the ends of a microtubule? We calculated the average length scanned by MCAK during a diffusive interaction with a microtubule to be 0.79 μm, calculated as $\sqrt{(2D\langle t \rangle)}$. This length of microtubule adjacent to the end acts as an 'antenna' for MCAK molecules (see Supplementary Information 2). To estimate the flux of MCAK to the microtubule end, we write[20]

$$\frac{\partial c}{\partial t} = k_{on}C_m - k_{off}c + D\frac{\partial^2 c}{\partial x^2}$$

where $c(x,t)$ is the concentration of MCAK on the microtubule lattice at distance x from the microtubule end and time t, k_{on} is the attachment rate to the lattice, C_m is the MCAK concentration in solution, and k_{off} is the dissociation rate from the lattice. This equation excludes the contribution of the depolymerization rate, which is negligible. The steady-state solution of this equation is given by $c(x) = c_\infty(1 - e^{-x/x_0})$, where c_∞ is the concentration on the microtubule lattice far from the end, in MCAK dimers per μm, and $x_0 = \sqrt{(D/k_{off})}$. The flux to the microtubule end is $J = -D\partial c/\partial x = -Dc_\infty/x_0$ (see Supplementary Information 3). c_∞ was measured for MCAK–GFP concentrations of 0.3–3 nM by direct counting of molecules. This allowed us to calculate the attachment rate to the microtubule lattice, $k_{on} = 0.64 \pm 0.13\,nM^{-1}\,s^{-1}\,\mu m^{-1}$ ($n = 3$). With this value of k_{on}, we calculated a flux to the end of the microtubule of 2.2 MCAK–GFP dimers per second at 6 nM, corresponding to an association rate to protofilament ends of $k_a = 26\,\mu M^{-1}\,s^{-1}$. Thus, the diffusion of MCAK accounts theoretically for the very high association rate measured in the initial-rate experiments (Fig. 1d).

Diffusive scanning followed by end capture was directly observed, as shown in Fig. 3a (yellow arrowhead). If an MCAK–GFP molecule lands within 0.25 μm of the microtubule end, it is likely to diffuse to the end within our 100-ms frame acquisition time; this accounts for end-binding events not preceded by observable diffusion

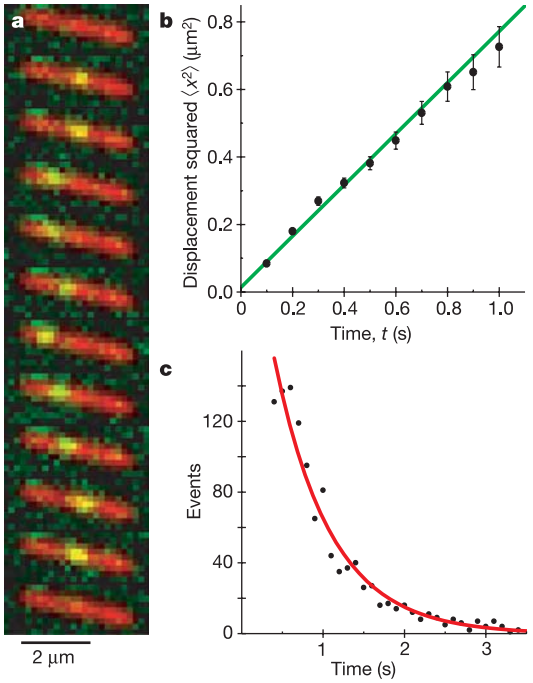

Figure 2 | MCAK–GFP diffusion along microtubules. a, Sequential frames of an MCAK–GFP (green) video. Twelve frames of a continuous TIRF-FITC recording (100-ms frames) were overlaid on one TRITC epifluorescence image of the microtubule (red). **b**, The mean-squared displacement of MCAK is plotted against the time interval over which it is measured. A linear curve fitted to the initial second yields a diffusion coefficient, D, of $0.38\,\mu m^2\,s^{-1}$; $\langle x^2 \rangle = 2Dt$. Error bars represent the s.e.m. of the squared displacement values. **c**, Histogram of durations of MCAK–GFP–microtubule interactions. An exponential curve fitted to the histogram (red) and corrected for photobleaching yields a mean lifetime of the interactions, $\langle t \rangle$, of 0.83 s.

(Fig. 3a, white arrowhead). Direct end binding from solution also occurs.

Why might MCAK use 1D diffusion instead of a directed walk to get to microtubule ends? One advantage is that, unlike directed motion, diffusion allows MCAK to target both ends of the microtubule, which is a significant feature of kinesin-13 localization *in vivo*[2,4]. A second advantage becomes clear when the diffusive movement of MCAK (with a diffusion coefficient of $0.38\,\mu m^2\,s^{-1}$) is compared with the directed movement of kinesin-1 (with a velocity of $0.8\,\mu m\,s^{-1}$)[19]: MCAK covers shorter distances more rapidly (Fig. 3b). For any distance shorter than 1 μm, MCAK will outpace kinesin-1 in a race to the microtubule end.

We found evidence that the rapid diffusion of MCAK to the microtubule end does indeed accelerate the depolymerization reaction. First, increasing the KCl concentration from 75 mM to 125 mM greatly decreased the lifetime of MCAK on the microtubule lattice and decreased the depolymerization rate to baseline levels (Fig. 3c and Supplementary Information 4). Because a high salt concentration may disrupt direct end association as well as lattice diffusion, we did a second experiment in which the negatively charged carboxy termini of tubulin, known as the 'E-hook'[21], was removed by digestion with subtilisin. This prevented MCAK from diffusing on the lattice (Fig. 3d, e) and significantly decreased the depolymerization rate to 26 ± 3% of control microtubules ($P < 0.1\%$, Welch's *t*-test), as shown previously with microtubule sedimentation assays[12,13]. Direct end binding still occurred, and nearly maximum depolymerization rates were observed when using very high concentrations of MCAK (Supplementary Information 4). Therefore the decrease in depolymerization rate for subtilisin microtubules is best explained by a decrease in end-targeting caused by the lack of E-hook-mediated diffusion.

The electrostatic partner for the negatively charged E-hook is probably the positively charged 'neck' domain[22], which has been shown to be necessary for MCAK depolymerization activity *in vivo*[23]. Complementing earlier work showing that electrostatic interactions of positively charged regions of kinesin-1 (refs 24, 25) and kinesin-3 (ref. 26) with the E-hook enhance processivity of directed motility, our results indicate that these interactions are important for diffusive motility as well. Taken together, these data connect diffusion and depolymerization: electrostatic interactions between MCAK's neck domain and the E-hook of tubulin give rise to diffusion and accelerated depolymerization.

ATP is hydrolysed while MCAK interacts with the lattice of microtubules[8]. It is clear that each individual diffusive step does not require ATP hydrolysis, because MCAK's lattice-stimulated ATPase activity was previously measured to be only $1\,s^{-1}$ (ref. 8), much lower than the rate of diffusive stepping ($12{,}000\,s^{-1}$). The mean interaction time of 0.83 s indicates that one diffusive interaction corresponds to one ATP hydrolysis cycle.

To determine whether diffusion depended on MCAK's nucleotide state, we performed single-molecule diffusion experiments with ADP, AMP-PNP (a non-hydrolysable ATP analogue) or apyrase (to digest all residual ATP and ADP) to mimic the ADP, ATP or

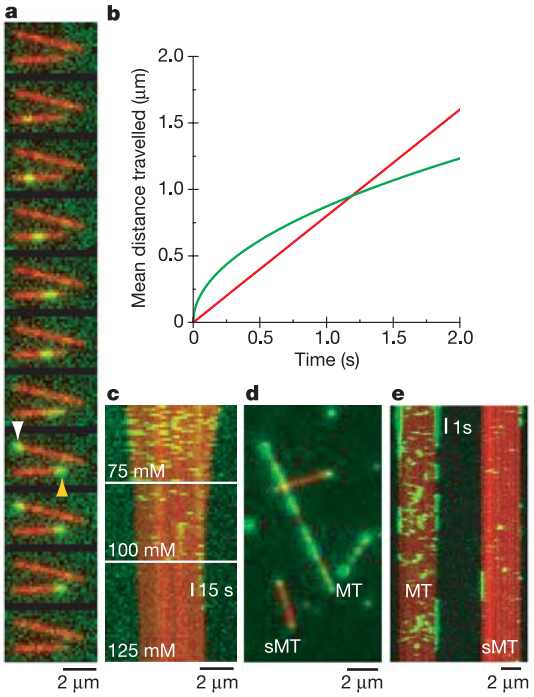

Figure 3 | MCAK targeting of microtubule ends by means of diffusion. **a**, Two MCAK–GFP molecules (green) interacting with separate microtubules (red) in 1 mM ATP (100-ms frames). Arrowheads indicate MCAK–microtubule end-binding events. **b**, Plot of average distance travelled over time by diffusing MCAK–GFP (green, $D = 0.38\,\mu m^2\,s^{-1}$; $\langle x \rangle = \sqrt{(2Dt)}$) and walking kinesin-1 (red, velocity $v = 0.8\,\mu m\,s^{-1}$; $\langle x \rangle = vt$). **c**, Kymograph showing the effect of KCl concentration on the MCAK interaction with a single microtubule. Microtubules are depicted along the horizontal axis while time changes along the vertical axis. The MCAK and MCAK–GFP concentrations were 2.5 and 0.25 nM, respectively. **d**, Dual-colour image of normal microtubules (MT) and subtilisin-digested microtubules (sMT) in the presence of 3 nM MCAK–GFP (green). **e**, Kymographs showing diffusion on a normal microtubule (MT) and only brief binding/unbinding events on a subtilisin-digested microtubule (sMT) at about 1 nM MCAK–GFP.

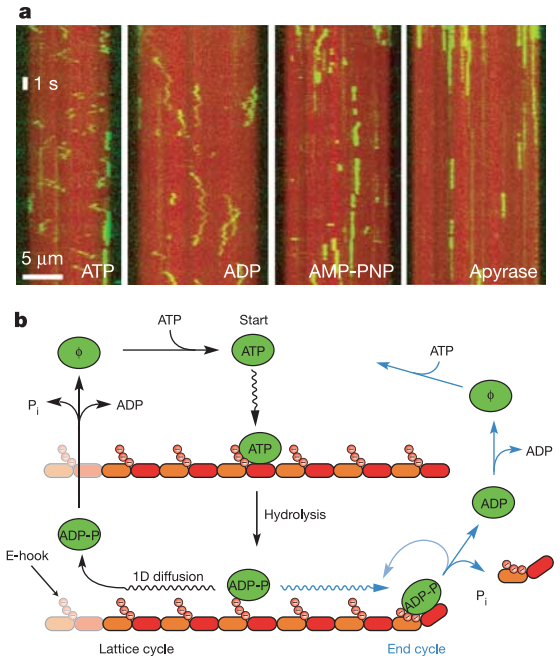

Figure 4 | MCAK nucleotide states and diffusion model. **a**, Kymographs depicting the motion of MCAK–GFP (green) along microtubules (red) in the presence of ATP (1 mM), ADP (1 mM), AMP-PNP (1 mM) and apyrase. The MCAK–GFP concentration was 0.6 nM except with apyrase, when it was 20 pM. **b**, MCAK–microtubule interaction model. Binding of soluble MCAK-ATP (green) induces rapid hydrolysis, accounting for the lattice-stimulated ATPase activity[8]. Next, MCAK-ADP-P_i diffuses along the lattice by means of the E-hook of tubulin. It may disassociate, 'unproductively' completing the hydrolysis cycle (left, black arrows). Alternatively, it may reach a microtubule end, where the removal of tubulin dimers is coupled to P_i release (right, blue arrows), accounting for the end-stimulated ATPase activity[8]. MCAK may detach from the end (straight blue arrow) or, if processive, may stay attached to remove additional dimers (light blue arrow).

nucleotide-free states, respectively. In 1 mM ADP, MCAK–GFP bound microtubules and moved in a diffusive manner ($D = 0.22 \pm 0.01\,\mu m^2\,s^{-1}$, $\langle t \rangle = 1.75 \pm 0.06$ s, $n = 1{,}076$) proving that diffusion occurred without energy derived from the hydrolysis of ATP (Fig. 4a, and Supplementary movie 3). Similar diffusion coefficients were measured in 0.1 and 10 mM ADP. The statistically significant difference in diffusion parameters (D and $\langle t \rangle$) in ADP compared with ATP implies that, in the presence of ATP, MCAK does not primarily diffuse in the ADP state. MCAK-AMP-PNP could bind to microtubules but only rarely showed diffusive steps ($D = 0.014\,\mu m^2\,s^{-1}$, $\langle t \rangle = 3.5$ s). When apyrase was added to remove both ATP and ADP from solution enzymatically, nucleotide-free MCAK–GFP went into a rigor state with greatly reduced diffusion ($D = 0.003\,\mu m^2\,s^{-1}$, $\langle t \rangle = 3.9$ s).

In the presence of ATP, MCAK must diffuse in one or more of the four possible nucleotide states: nucleotide-free, ATP, ADP and ADP-P_i. As MCAK binds tightly in the presence of AMP-PNP and apyrase, both the ATP and nucleotide-free states are excluded. Because the diffusion observed in ADP is statistically distinct from that observed in ATP, MCAK apparently diffuses in the ADP-P_i state. To induce an ADP-P_i-like state, we performed a single-molecule diffusion experiment in ADP·AlF_x, ADP·BeF_x and ADP·vanadate. Diffusion was observed in all three cases (Supplementary Information 5). The results imply that MCAK normally, in the presence of ATP, diffuses in the ADP-P_i state.

In what nucleotide state is MCAK when it first encounters the microtubule? To determine the nucleotide state of soluble MCAK, we measured the amounts of radiolabelled α- and γ-phosphates of ATP bound to MCAK and kinesin-1 free in solution without microtubules (Supplementary Information 5). As shown previously[27], no γ-P_i was bound to kinesin (γ-P_i/α-P_i = −11 ± 8% in two experiments). However, equal amounts of α-P_i and γ-P_i remained bound to MCAK (γ-P_i/α-P_i = 116 ± 11% in three experiments). This shows that MCAK exists in the ATP or ADP-P_i state in solution, unlike kinesin-1, and indicates that the functional differences between kinesin-1 and kinesin-13 family proteins are achieved through differences in hydrolysis mechanisms. The nucleotide data were used to formulate a MCAK–microtubule interaction model that accounts for both the microtubule lattice-stimulated and end-stimulated ATPase activity of MCAK (Fig. 4b).

After arriving at the end, each MCAK seems to remove several dimers. Comparison of the flux to the microtubule end calculated theoretically (2.2 MCAK dimers per second at 6 nM) with the off-rate of tubulin dimers ($14\,s^{-1}$ at 6 nM MCAK–GFP) indicates that each MCAK removes about seven tubulin dimers for each end-targeting event. On average, single MCAK end-binding events were observed to last 1.9 ± 0.2 s ($n = 239$, corrected for photobleaching). At saturating concentration, MCAK removes tubulin dimers from protofilaments at a rate of two dimers per second, so an MCAK that resides for 1.9 s at an end would remove about four tubulin dimers. Taken together, these results indicate that MCAK might act processively at the microtubule end.

By diffusing along microtubules instead of walking, MCAK rapidly targets both microtubule ends. A comparable process is the rapid targeting of DNA restriction enzymes to their restriction sites, which also exceeds the three-dimensional diffusion limit[28]. These DNA enzymes are thought to target their restriction sites by a 1D diffusional scan of DNA segments[29,30], but this search mechanism has not been observed at the single-molecule level. Here we have characterized the 1D diffusion of MCAK on microtubules and shown the implications of this diffusion for end targeting. The single-molecule data presented here support the 'reduction in dimensionality' hypothesis.

The MCAK neck domain data[23] suggest that 1D diffusion operates *in vivo* to target MCAK to microtubule ends. Once at the ends, MCAK and its homologues interact with other proteins, such as the plus-end-binding proteins XMAP215 and EB1 (refs 6, 7), to regulate microtubule dynamics. The *in vitro* single-molecule approach taken here could be useful to study the dynamics of this molecular machinery.

METHODS

Proteins. Human MCAK–His_6 and human MCAK–His_6 tagged with enhanced GFP were expressed in *Spodoptera frugiperda* (Sf9) cells (BAC-TO-BAC expression system; Invitrogen) and purified by cation-exchange, metal-chelating, and desalting or gel-filtration chromatography. Most experiments with MCAK–GFP were performed with freshly purified protein. A filter-based radiometric ATP binding assay[8] with [γ-^{32}P]ATP and [α-^{32}P]ATP was used to determine the concentration of active MCAK and the nucleotide state of proteins in solution. Details are given in Supplementary Information 5 and 6. Reagents were purchased from Sigma unless indicated otherwise. Pig-brain tubulin was purified, rhodamine-labelled (TAMRA; Invitrogen) and polymerized with GMP-CPP (Jena Bioscience) as described previously[8]. Key experiments were repeated with Taxol-stabilized microtubules; no differences were observed. Digestion was performed with $10\,\mu g\,ml^{-1}$ subtilisin, incubated for 20 min at 37 °C, and terminated with 2 mM phenylmethylsulphonyl fluoride.

Imaging. Images were acquired with either a Roper Scientific MicroMAX:512BFT charge-coupled device camera or an Andor DV887 iXon camera with Zeiss Axiovert 200M microscopes and Zeiss 100 × /1.45 α Plan-FLUAR objectives. The microscopes were outfitted with a dual-port TIRF condenser (Till Photonics) or a prototype VisiTIRF condenser (Visitron Systems). Fluorescein isothiocyanate (FITC) and tetramethylrhodamine β-isothiocyanate (TRITC) filter sets (Chroma Technology Corp.) were used to image GFP (TIRF) and TAMRA (epifluorescence) fluorophores, respectively. The standard exposure time was 100 ms.

Depolymerization assay. Microscope chambers were constructed with 18 mm × 18 mm and 22 mm × 22 mm coverslips separated by double-sided tape (Scotch 3M) to create channels 0.1 mm thick, 3 mm wide and 18 mm long. Glass coverslips (no. 1.5; Corning) were cleaned in Pirnaha solution (H_2O_2/H_2SO_4, 3:5) before silanization in 0.05% dichlorodimethylsilane in trichloroethylene. Detailed methods are given in Supplementary Information 6. To immobilize microtubules, channels were incubated with 0.2% Tub 2.1 antibody in BRB80 for 5 min, followed by 5 min with 1% Pluronic F-127 in BRB80, and finally GMP-CPP microtubules in BRB80 for 15 min. Channels were rinsed with BRB20 (20 mM PIPES-/KOH pH 6.9, 1 mM $MgCl_2$, 1 mM EGTA) before addition of the imaging solution (BRB20 supplemented with 75 mM KCl, $0.1\,mg\,ml^{-1}$ BSA, 1 mM ATP or other nucleotides, 1% 2-mercaptoethanol, 40 mM glucose, $40\,\mu g\,ml^{-1}$ glucose oxidase, $16\,\mu g\,ml^{-1}$ catalase, and MCAK).

Imaging analysis. The Motion Tracking software package, written in the Pluk development environment, was used to locate and track MCAK–GFP molecules[18]. The validity of each track was confirmed by visual inspection. The Pluk-derived diffusion coefficient was cross-checked against, first, trajectories generated by hand with kymographs and a custom MATLAB-based two-dimensional gaussian peak-fitting tool, and second, an analysis of displacement distributions that does not require manual inspection. Details are given in Supplementary Information 1. For each condition examined, at least three separate experiments were performed, and multiple films of each experiment were analysed, yielding no less than 100 molecules.

Received 16 February; accepted 17 March 2006.

1. Desai, A., Verma, S., Mitchison, T. J. & Walczak, C. E. Kin I kinesins are microtubule-destabilizing enzymes. *Cell* **96**, 69–78 (1999).
2. Maney, T., Hunter, A. W., Wagenbach, M. & Wordeman, L. Mitotic centromere-associated kinesin is important for anaphase chromosome segregation. *J. Cell Biol.* **142**, 787–801 (1998).
3. Rogers, G. C. *et al.* Two mitotic kinesins cooperate to drive sister chromatid separation during anaphase. *Nature* **427**, 364–370 (2004).
4. Walczak, C. E., Mitchison, T. J. & Desai, A. XKCM1: a *Xenopus* kinesin-related protein that regulates microtubule dynamics during mitotic spindle assembly. *Cell* **84**, 37–47 (1996).
5. Homma, N. *et al.* Kinesin superfamily protein 2A (KIF2A) functions in suppression of collateral branch extension. *Cell* **114**, 229–239 (2003).
6. Tournebize, R. *et al.* Control of microtubule dynamics by the antagonistic activities of XMAP215 and XKCM1 in *Xenopus* egg extracts. *Nature Cell Biol.* **2**, 13–19 (2000).
7. Mennella, V. *et al.* Functionally distinct kinesin-13 family members cooperate to regulate microtubule dynamics during interphase. *Nature Cell Biol.* **7**, 235–245 (2005).
8. Hunter, A. W. *et al.* The kinesin-related protein MCAK is a microtubule depolymerase that forms an ATP-hydrolyzing complex at microtubule ends. *Mol. Cell* **11**, 445–457 (2003).

9. Wordeman, L. & Mitchison, T. J. Identification and partial characterization of mitotic centromere-associated kinesin, a kinesin-related protein that associates with centromeres during mitosis. *J. Cell Biol.* **128,** 95–104 (1995).
10. Adam, G. & Delbruck, M. in *Structural Chemistry of Molecular Biology* (eds Rich, A. & Davidson, N.) 198–215 (Freeman, San Francisco, 1968).
11. Richter, P. H. & Eigen, M. Diffusion controlled reaction rates in spheroidal geometry. Application to repressor–operator association and membrane bound enzymes. *Biophys. Chem.* **2,** 255–263 (1974).
12. Moores, C. A. *et al.* A mechanism for microtubule depolymerization by KinI kinesins. *Mol. Cell* **9,** 903–909 (2002).
13. Niederstrasser, H., Salehi-Had, H., Gan, E. C., Walczak, C. & Nogales, E. XKCM1 acts on a single protofilament and requires the C terminus of tubulin. *J. Mol. Biol.* **316,** 817–828 (2002).
14. Mandelkow, E. M., Mandelkow, E. & Milligan, R. A. Microtubule dynamics and microtubule caps: a time-resolved cryo-electron microscopy study. *J. Cell Biol.* **114,** 977–991 (1991).
15. Hyman, A. A., Salser, S., Drechsel, D. N., Unwin, N. & Mitchison, T. J. Role of GTP hydrolysis in microtubule dynamics: information from a slowly hydrolyzable analogue, GMPCPP. *Mol. Biol. Cell* **3,** 1155–1167 (1992).
16. Northrup, S. H. & Erickson, H. P. Kinetics of protein–protein association explained by Brownian dynamics computer simulation. *Proc. Natl Acad. Sci. USA* **89,** 3338–3342 (1992).
17. Howard, J. *Mechanics of Motor Proteins and the Cytoskeleton* (Sinauer, Sunderland, Massachusetts, 2001).
18. Kalaidzidis, Y. L., Gavrilov, A. V., Zaitsev, P. V., Kalaidzidis, A. L. & Korolev, E. V. PLUK—an environment for software development. *Program. Comput. Softw.* **23,** 206–211 (1997).
19. Howard, J., Hudspeth, A. J. & Vale, R. D. Movement of microtubules by single kinesin molecules. *Nature* **342,** 154–158 (1989).
20. Klein, G. A., Kruse, K., Cuniberti, G. & Julicher, F. Filament depolymerization by motor molecules. *Phys. Rev. Lett.* **94,** 108102 (2005).
21. Paschal, B. M., Obar, R. A. & Vallee, R. B. Interaction of brain cytoplasmic dynein and MAP2 with a common sequence at the C terminus of tubulin. *Nature* **342,** 569–572 (1989).
22. Maney, T., Wagenbach, M. & Wordeman, L. Molecular dissection of the microtubule depolymerizing activity of mitotic centromere-associated kinesin. *J. Biol. Chem.* **276,** 34753–34758 (2001).
23. Ovechkina, Y., Wagenbach, M. & Wordeman, L. K-loop insertion restores microtubule depolymerizing activity of a 'neckless' MCAK mutant. *J. Cell Biol.* **159,** 557–562 (2002).
24. Thorn, K. S., Ubersax, J. A. & Vale, R. D. Engineering the processive run length of the kinesin motor. *J. Cell Biol.* **151,** 1093–1100 (2000).
25. Wang, Z. & Sheetz, M. P. The C-terminus of tubulin increases cytoplasmic dynein and kinesin processivity. *Biophys. J.* **78,** 1955–1964 (2000).
26. Nitta, R., Kikkawa, M., Okada, Y. & Hirokawa, N. KIF1A alternately uses two loops to bind microtubules. *Science* **305,** 678–683 (2004).
27. Hackney, D. D. Kinesin ATPase: Rate-limiting ADP release. *Proc. Natl Acad. Sci. USA* **85,** 6314–6318 (1988).
28. Riggs, A. D., Bourgeois, S. & Cohn, M. The lac repressor–operator interaction. 3. Kinetic studies. *J. Mol. Biol.* **53,** 401–417 (1970).
29. Winter, R. B., Berg, O. G. & von Hippel, P. H. Diffusion-driven mechanisms of protein translocation on nucleic acids. 3. The *Escherichia coli* lac repressor–operator interaction: kinetic measurements and conclusions. *Biochemistry* **20,** 6961–6977 (1981).
30. Halford, S. E. & Marko, J. F. How do site-specific DNA-binding proteins find their targets? *Nucleic Acids Res.* **32,** 3040–3052 (2004).

Supplementary Information is linked to the online version of the paper at www.nature.com/nature.

Acknowledgements We thank R. Hartmann for cloning and protein purification work; V. Varga for purification of unlabelled MCAK; E. Schäffer for the application of F-127; F. Ruhnow for the two-dimensional gaussian peak-fitting tool; A. Hyman, F. Jülicher, E. Schäffer, I. Riedel, J. Stear, G. Klein, V. Varga, A. Hunt and H. T. Schek for review of the manuscript; and S. Wolfson for proofreading and editing. Andor Technologies lent us the Andor iXon camera, and the VisiTIRF condenser was developed in collaboration with Visitron Imaging Systems, GmbH. This research was supported by the Max Planck Gesellschaft and the NIH.

Author Information Reprints and permissions information is available at npg.nature.com/reprintsandpermissions. The authors declare no competing financial interests. Correspondence and requests for materials should be addressed to J.H. (howard@mpi-cbg.de).

Supplementary Information for "The depolymerizing kinesin MCAK uses lattice diffusion to rapidly target microtubule ends"

Jonne H. Helenius[1⋆], Gary J. Brouhard[1⋆], Yannis Kalaidzidis[1,2], Stefan Diez[1], and Jonathon Howard[1]

Contents

1 Calculating Diffusion

1.1 Image processing

Movies of MCAK-GFP diffusion were analyzed using "Motion Tracking," an in-house software package written in the Pluk software development environment (ref. 18). The program starts by identifying peaks in the pixel intensity values for a single frame of the movie. Intensity peaks are assigned (x, y) position values by fitting the experimental intensity distribution with a squared Lorentzian function. In this way, each frame is described by a sum of squared Lorentzian functions:

$$I(x,y) = \sum_i \frac{A_i}{1 + \left\{ \frac{(x-x_i)^2 + (y-y_i)^2}{w_i^2} \right\}^2} + B(x_i, y_i) \quad \text{(S1)}$$

where A_i is the intensity of the i-th particle, (x_i, y_i) are the i-th particle's center coordinates, w_i is the width of the i-th particle by two perpendicular dimensions, and $B(x_i, y_i)$ is the residue of background in the vicinity of the i-th particle. From the sequence of frames, the noise is modeled by:

$$\mathcal{N}(x,y) = \alpha \cdot I(x,y) + \mathcal{N}_0 \quad \text{(S2)}$$

where $\mathcal{N}(x, y)$ is the noise variance in point (x, y), α is the scaling factor for Poisson noise, $I(x, y)$ is the intensity in point (x, y), and $\mathcal{N}_0$ is the intensity-independent noise minus the offset in the intensity counts. Intensity peaks that overcame the threshold $4\sqrt{\mathcal{N}(x,y)}$ were retained. For each intensity peak, the program calculates the position (x_i, y_i), size (w_i), and mean and integral intensity. Next, the program examines subsequent movie-frames, and links the positions of individual molecules located on a microtubule together into trajectories, or tracks. The minimum track length was kept at 4 frames, which was 400 ms for our 100 ms exposure time.

The program occasionally errs in constructing a molecule trajectory and/or follows a clearly stationary molecule. Therefore, each track generated by the computer program is manually inspected. Tracks were excluded from the analysis if any of the following conditions occurred: (a) the track remained stationary, (b) the track jumped between neighboring microtubules, (c) the track dwelled at the end of a microtubule, (d) the track switched between diffusive movement and clearly stationary binding, or (e) the tracks of adjacent molecules overlapped, creating the possibility that the program confused the tracks after the encounter. The manual grooming process typi-

[1]Max Planck Institute of Molecular Cell Biology and Genetics, Pfotenhauerstraße 108, 01307 Dresden, Germany, [2]A. N. Belozersky Institute of Physico-Chemical Biology, Moscow State University, Moscow 119899, Russia.
⋆These authors contributed equally to this work.

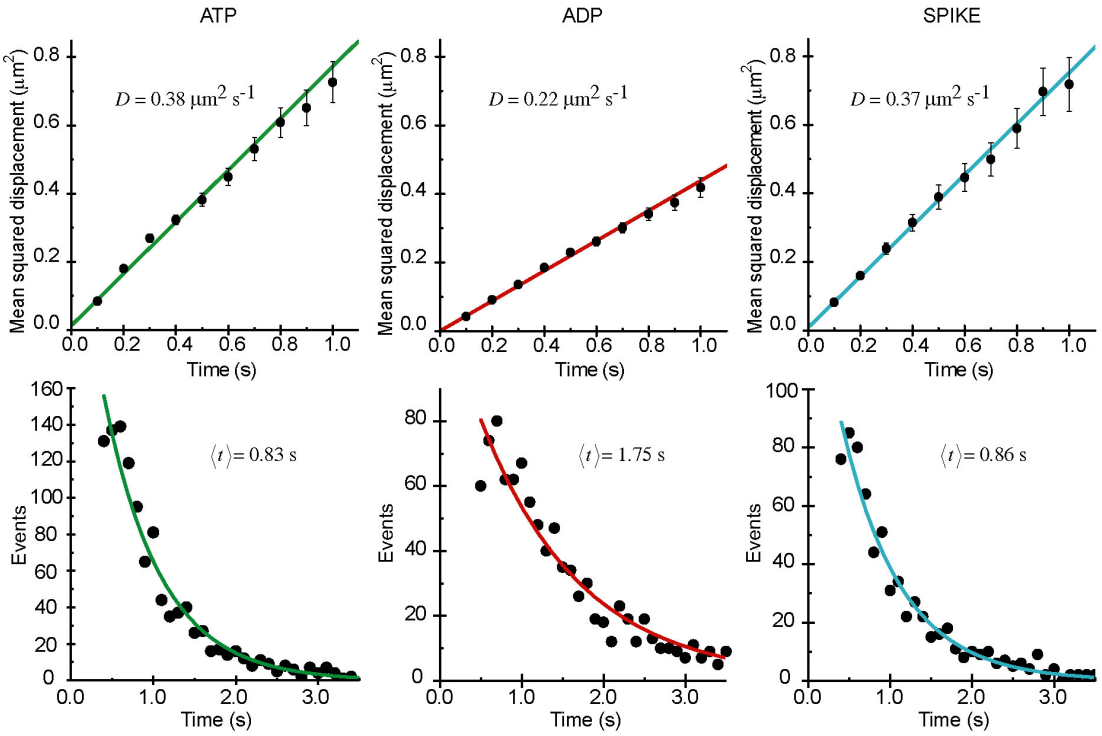

Figure S1 | Diffusion Data for 3 conditions. On top, the mean-squared displacement versus time plots used to calculate the diffusion coefficient. On bottom, the distribution of interaction times used to calculate the mean lifetime. The mean lifetimes specified were corrected for photobleaching (see below).

cally excluded 20-40% of the initial output from the Motion Tracking program. Most of the excluded tracks were stationary particles (condition (a) above) that could be MCAK molecules stuck to the coverglass surface near microtubules, dead MCAKs bound irreversibly to the microtubule, or perhaps MCAKs trapped by defects in the microtubule lattice. The remaining tracks comprise the data set used for further analysis. The position data for all tracks were exported from Pluk into MATLAB (The Mathworks). In MATLAB, the track data from multiple movies were compiled into a data set, from which the $\langle x^2 \rangle$ versus time plot and the interaction time histogram are calculated. Regression analysis was carried out in Origin 7 (Rockware). The linear regression used a weighted least-squares algorithm, which did not include a point at $t = 0$ and was not force-fit through zero.

Does the diffusive behavior of MCAK change at high concentrations and depolymerization rates? At concentrations higher than 1.5 nM MCAK-GFP dimer, single molecule trajectories could no longer be discriminated, but very little depolymerization occurred at concentration lower than 1.5 nM. To increase depolymerization rates while allowing single molecules to be observed, we added both GFP-tagged and untagged MCAK in varying ratios, for total concentrations of 3-30 nM ("spike" experiments). In the presence of untagged MCAK, the behavior of GFP-tagged MCAK remained unchanged at all concentrations tested (combined result: $D = 0.37 \pm 0.02$ μm^2 s^{-1}, $\langle t \rangle = 0.86 \pm 0.04$ s, $n = 690$, see Fig. S1).

The diffusion coefficient in ATP was found to be equivalent between two different experimenters (J.H.H. and G.J.B), over 16 experiments, using MCAK proteins from 3 separate protein purifications. For the other conditions described, at least three separate experiments were performed. As stated above, the manual inspection of tracks typically excluded 20-40% of the initial output from the Motion Tracking program. To rule out the possibility of a strong bias in our manual grooming of track data, an entirely computer-based cross-check of the diffusion calculation was performed. Initially, the Motion Tracking software found tracks for both moving and stationary signals, after which we normally removed tracks not consistent with diffusion (see above). Instead, all tracks were used to generate a distribution of displacements over discrete time segments. Each track was broken into multiple independent segments, e.g., a 4 s trajectory yields 39 $\times$ 0.1 s segments or 3 $\times$ 1.1 s segments. According to 1-D diffusion theory, the distribution of distances traveled for a given time is a Gaussian function, whose width is related to the diffusion coefficient (ref. S1). As we expect to have two distinct populations of molecules, those diffusing and those stationary, the sum of two Gaussian functions should describe the experimental distributions. Indeed, we found a narrow Gaussian, representing stationary behavior, and a

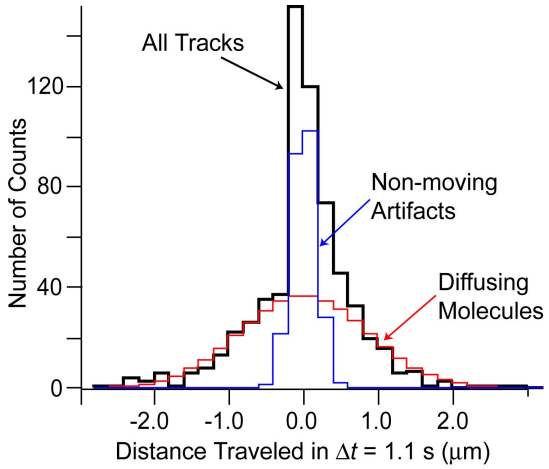

Figure S2 | Distribution of Distance Traveled. The Motion Tracking software package found a distribution of the distance traveled by all tracked particles over time segments of $\Delta t = 1.1$ s of elapsed time (black histogram). The histogram was fit with the sum of two Gaussian distributions corresponding to (a) stationary particles (blue histogram) and (b) diffusing particles (red histogram). In this example, the non-moving artifacts comprised 32.5% of the tracks and included MCAKs bound to the coverglass surface, dead MCAKs stuck irreversibly to the microtubule, and automated tracking artifacts.

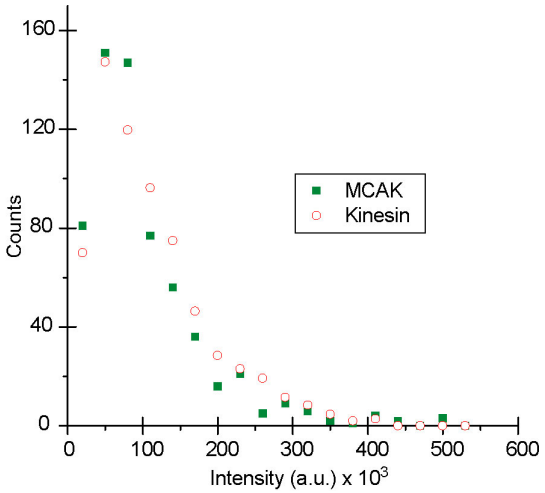

Figure S3 | Distribution of Molecule Intensities. The histogram compares the intensity distributions of MCAK-GFP and GFP-tagged kinesin-1 molecules imaged simultaneously. The distribution of MCAK-GFP intensities is shown in green. The distribution of GFP-tagged kinesin-1 intensities is shown in red.

second, broad Gaussian, indicating diffusive behavior with a diffusion coefficient of 0.37 μm^2 s^{-1} (for an example, see Figure S2). This is statistically equivalent to our earlier data. Therefore, we conclude that our manual inspection procedure successfully excludes stationary particles without introducing bias, and manually-groomed data is used in all further analysis.

1.2 The tracked molecules are single MCAK dimers

Like many kinesins, MCAK is thought to form a homo-dimer (ref. 2). The fluorescent signals we tracked should thus have been MCAK-GFP homo-dimers. How do we know we are observing single MCAK homo-dimers and not aggregated multimers? Three observations support the argument for single molecules. First, the purified protein eluted from the gel filtration column as a clear, single peak indicative of a homogenous population. We performed all critical experiments using freshly-purified protein, because frozen protein forms aggregates which exhibit odd behaviors and confound analysis. Second, two GFP fluorophores bound to the same molecule should undergo a two-step photobleaching process: the emitted light level, initially high, drops to an intermediate level before extinguishing completely. This type of behavior was recorded for multiple MCAK-GFP molecules. However, the majority of molecules dissociate from the microtubule before a bleaching event occurs. In addition, the blinking of GFP and the heterogeneity between individual GFP moieties did not allow good numerical quantification of the bleaching, and only a fraction of tracked molecules showed clear two-step bleaching. Finally, comparing the MCAK-GFP signal with that of GFP-tagged kinesin-1 provided conclusive evidence that we were observing MCAK homo-dimers. Both molecules were allowed to move along microtubules at the same time while imaged in the single molecule microscope assay. The tracks of GFP molecules were readily categorized into those that moved in a continuous directed manner (kinesin-1) and those that diffused along the microtubules (MCAK). A histogram of the intensity of the light measured for the signals associated with both type of tracks is shown in Supplementary Fig. 3. The kinesin-1 population is known to exist as homo-dimers from an analysis of run-lengths, which correspond to well-established values for single kinesin motors.

1.3 Correction for photobleaching

As shown in Fig. 2c of the main text and Fig. S1, the lifetimes of MCAK-microtubule interactions decay exponentially. The observed exponential decay, with a time constant of the decay, $\tau_{\rm obs}$, is actually the combination of two processes: (a) the dissociation of MCAK from the microtubule and (b) the bleaching of GFP fluorophores on MCAK molecules. The time constants of these two processes are related to the observed time constant by:

$$\frac{1}{\tau_{\rm obs}} = \frac{1}{\tau_{\rm B}} + \frac{1}{\tau_{\rm D}} \qquad \text{(S3)}$$

where $\tau_{\rm D}$ is the time constant of MCAK dissociation and $\tau_{\rm B}$ is the time constant of bleaching. The time constant of bleaching was measured for stationary MCAK-GFP molecules that non-specifically adhered to the cover-slip surface. The number of molecules observed on the surface

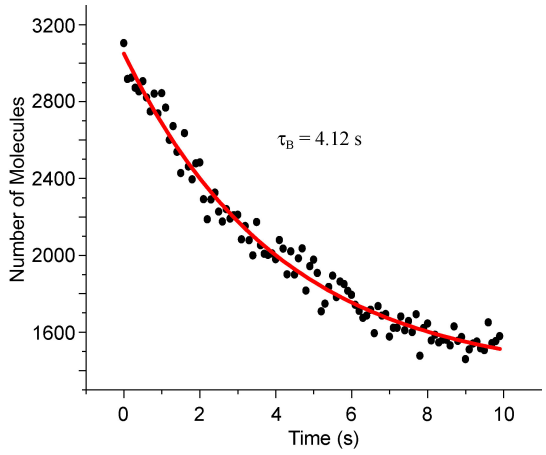

Figure S4 | Distribution of Surface-Bound Molecules over Time. The number of surface-bound molecules observed (black dots) decays exponentially as the GFP-moieties are bleached. An exponential decay fit (red line) gives a time constant, τ_B, of 4.12 s.

decayed exponentially as the GFP moieties bleached (Fig. S4). The time constant of bleaching was found to be τ_B = 4.12 s. This value was used to calculate τ_D, the mean lifetimes reported in the main text.

1.4 Directional bias

We tested for the presence of directional bias in our data by fitting the $\langle x^2 \rangle$ values to the equation for diffusion plus directed motion: $\langle x^2 \rangle = 2Dt + vt^2$, where v is the velocity of directed motion. The polynomial regression produces a negative value for v, which is nonsensical; the polynomial slopes in the opposite direction from the expected curve. From the regression results, we can state with 98.6% confidence that v is ≤ 0.1 μm s^{-1}.

2 Lattice vs. End Targeting from Solution

How much better a target is the microtubule lattice than its ends? For simplicity, we can consider the microtubule end to be an absorbing disk and the microtubule to be a long cigar shaped ellipsoid. The flux (J_d) to a disk of radius r_d is

$$J_d = 4D_3 r_d C_0 \tag{S4}$$

where D_3 is the diffusion coefficient of the molecule in solution and C_0 is its concentration at distance ∞ from the disk (Sup. Ref. 1). The flux (J_e) to an absorbing cigar-shaped ellipsoid with long-axis $l \gg r_1 = r_2$ is

$$J_e = \frac{4\pi D_3 l C_0}{\ln(2l/r_1)} \tag{S5}$$

If we set r_d and r_1 equal to the radius of a microtubule, 12.5 nm, and l equal to the length of a microtubule that acts as an antenna, x_{RMS} = 790 nm, then J_e is over 40 times greater than J_d. In other words, a molecule diffusing in solution is 40 times more likely to hit the lattice than the end.

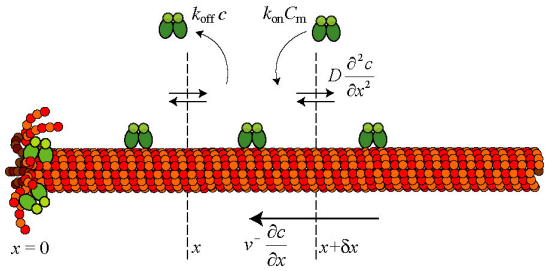

Figure S5 | Diagram of the mass transfer differential equation model. MCAK molecules (green) are shown attaching to the microtubule (red), detaching from the microtubule, and diffusing. These events change the concentration of MCAK molecules along the length $x \rightarrow x + \delta x$.

3 Mass Transfer Differential Equation Model

The mass transfer differential equation model is a simplified version of the equations published by Klein, et al. (ref. 20). The simplified model treats the microtubule end as an infinite sink for the absorption of MCAK molecules. In contrast, the complete Klein, et al. model considers the residence time of MCAK at the microtubule end, the processivity of the motor, and the availability of end-binding sites when neighboring MCAKs are present. The present model reduces the complexity in order to calculate the flux of MCAK molecules to the microtubule end, regardless of the behavior of MCAK upon reaching the end. If $c(x,t)$ is the concentration of MCAK on the microtubule lattice at position x from the microtubule end and time t, when we expect that $c(x,t)$ obeys the mass transfer equation:

$$\frac{\partial c}{\partial t} = k_{on}C_m - k_{off}c + D\frac{\partial^2 c}{\partial x^2} + v^- \frac{\partial c}{\partial x} \tag{S6}$$

where k_{on} is the attachment rate to the microtubule lattice, k_{off} is the dissociation rate from the lattice, C_m is the MCAK concentration in solution, D is the diffusion coefficient on the microtubule lattice, and v^- is the depolymerization rate (Fig. S5).

We specify the following boundary conditions:
(a) $c(x = 0) = 0$(infinite sink at the microtubule end),
(b) $c(x \rightarrow \infty) = k_{on}C_m/k_{off} = c_\infty$,
(c) $\partial c/\partial t = 0$ (steady state assumption).

We also assume a negligible speed for v^- (in μm·s^{-1}). Then, the mass transfer equation has the solution:

$$c(x) = c_\infty \left(1 - e^{-x/x_0}\right) \tag{S7}$$

where $x_0 = \sqrt{D/k_{off}}$. From this equation, we can calculate the flux, J, using Fick's first equation, $J = -D \cdot \partial c/\partial x$.

Table S1 | Parameters for the mass transfer model. The concentration C_m was derived from the radiometric assay (see below).

k_{on}	on-rate to the lattice	0.64 ± 0.13 nM^{-1}s^{-1} μm^{-1}
k_{off}	off-rate from the lattice	1.21 s^{-1}
D	1D diffusion coefficient	0.38 μm^2 s^{-1}

At $x = 0$,

$$J_0 = -Dc_\infty/x_0 \quad \text{(S8)}$$

Therefore, to calculate the flux to the end, we must measure D, k_{off}, and c_∞. The value of D is 0.38 μm^2 s^{-1}, and k_{off} is the inverse of the mean interaction time with the lattice ($\langle t \rangle^{-1} = 1.21$ s^{-1}). The value of c_∞ can be measured for MCAK concentrations of 0.3-3 nM by direct counting of particles. This allowed us to calculate the attachment rate to the microtubule lattice, $k_{on} = 0.64 \pm 0.13$ nM^{-1} s^{-1} μm^{-1}. With this value of k_{on} and using Eq. S8, we calculated a flux to the end of the microtubule of 2.2 MCAK dimers s^{-1} at 6 nM, corresponding to an association rate to protofilament ends of $k_a = 26$ mM^{-1} s^{-1}. Thus, the diffusion of MCAK accounts theoretically for the very high association rate measured in the initial-rate experiments (Fig. 1d). The measured parameters are summarized in Table S1.

4 Salt Concentration and Subtilisin-digested Microtubule Experiments

Two treatments that interfere with diffusion lead to a decreased depolymerization rate, as predicted if the diffusion of MCAK to the microtubule end is the rate-limiting step. Diffusion is thought to occur through weak electrostatic interactions between MCAK and the microtubule (ref. 8). In support of the electrostatic-interaction hypothesis, the diffusion of MCAK on microtubules was not observed at non-physiological high salt concentrations. Kymographs in Figure 3 c show the effects of raising the KCl concentration on the interaction of MCAK molecules with a single microtubule. While the KCl concentration was raised from 75 to 100 and finally 125 mM, MCAK and MCAK-GFP concentrations were maintained at 2.5 nM and 0.25 nM, respectively. A mixture of MCAK and MCAK-GFP was used in order to induce depolymerization while also observing single molecules. Microtubule depolymerization rates were 0.77 ± 0.05 μm min^{-1} at 75 mM, 0.22 ± 0.07 μm min^{-1} at 100 mM and 0.03 ± 0.03 μm min^{-1} at 125 mM KCl ($n = 10$ in each case). Relative GFP signals on the microtubule lattice were 1.0, 0.23 and 0.06 at 75, 100, 125 mM KCl, respectively. A relatively minor increase in salt concentration greatly reduced MCAK binding to the microtubule lattice and blocked MCAK-dependent microtubule depolymerization.

However, it is possible that the high-salt condition inhibits depolymerization because it disrupts end-association and not just lattice diffusion. Therefore, to further test the hypothesis that diffusion accelerates depolymerization, we repeated our experiments using subtilisin-digested microtubules. MCAK was unable to diffuse on these microtubules. Instead, the protein only bound to the microtubule for brief periods, generally shorter than 100 ms (see Fig. 3d and 3e). The experiments with subtilisin-digested microtubules were performed at several MCAK concentrations. Without MCAK, subtilisin-digested microtubules showed the same baseline depolymerization rate as undigested microtubules (0.03 ± 0.01 μm min^{-1}) (see Figure S6 a). At MCAK concentrations of 1-20 nM, the subtilisin-digested microtubules depolymerized significantly slower than undigested control microtubules present in the same sample chamber (Figure S6 b). However, at very high MCAK concentrations (100 nM), well above the normal KM, the subtilisin digested microtubules depolymerized at rates nearly equivalent to normal microtubules (Figure S6 c).

From these results, we conclude that subtilisin digestion did not change the intrinsic stability of GMP-CPP microtubules in our assay. Furthermore, the fact that very high depolymerization rates were recovered at high concentrations of MCAK argues that subtilisin digestion does not inhibit the end-specific catalytic mechanism that results in the removal of tubulin dimers. Therefore, the reduction in depolymerization rate at concentrations near the normal KM (e.g., 3-10 nM) was explained by a reduction in the rate of end-targeting, caused by the absence of E-hook mediated diffusion. Only at very high MCAK concentrations was the rate of direct end-binding from solution sufficient to overcome the inability to diffuse along the lattice. The lack of complete recovery in depolymerization rate leaves open the possibility that the E-hook plays a minor role in end-specific events as well.

5 Nucleotide State Experiments

5.1 ADP-P_i analogue experiments

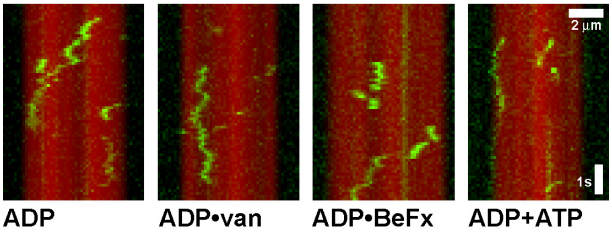

Figure S7 | MCAK diffusion in differing ADP nucleotide states. Kymographs showing the diffusion of MCAK-GFP along microtubules in differing nucleotide solutions: ADP (1 mM ADP), ADP·Van (1mM ADP, 2 mM Na_3VO_4), ADP·BeFx (1 mM ADP, 1 mM $BeCl_2$, 5 mM NaF) and ADP+ATP (1 mM ADP, 2 mM ATP). MCAK-GFP concentration, 0.5 nM, was kept the same.

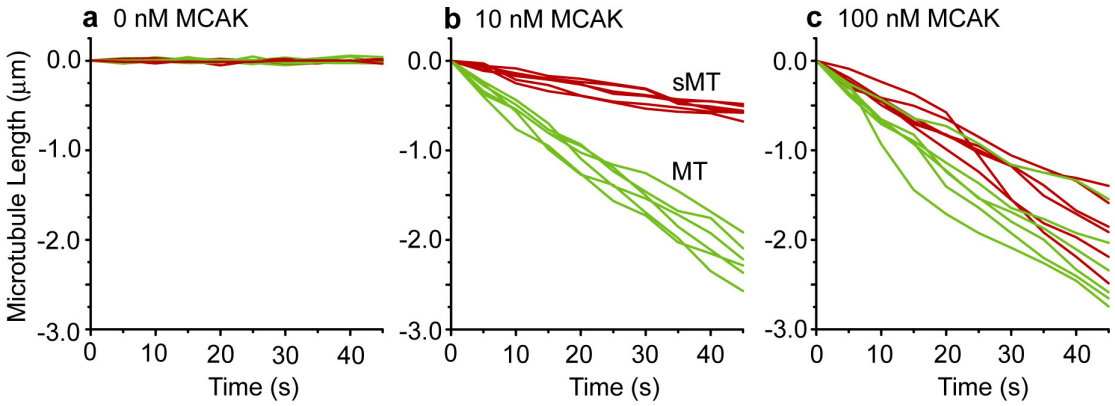

Figure S6 | Microtubule Depolymerization of Subtilisin-digested versus Control Microtubules. The three panels show normalized microtubule length versus time for 6 subtilisin digested microtubules (red) and 6 undigested control microtubules (green). The slope of these lines gives the depolymerization rate. **a**, 0 nM MCAK, showing baseline depolymerization. **b**, 10 nM MCAK, subtilisin digested microtubules depolymerized at 0.75 ± 0.04 μm min^{-1}, control microtubules depolymerized at 2.9 ± 0.2 μm/min. **c**, 100 nM MCAK, subtilisin digested microtubules depolymerized at 2.6 ± 0.2 μm min^{-1}, control microtubules depolymerized at 3.2 ± 0.3 μm min^{-1}.

5.2 Details regarding radiometric assay

Radiometric ATP binding assays (ref. 8) were performed in parallel using ATP labeled at either the α- or γ- phosphates. Briefly, proteins were incubated in labeling mix: BRB80 (80 mM PIPES-/KOH pH 6.9, 1 mM $MgCl_2$, 1 mM EGTA), 1 mg/ml BSA, and 13 mM ATP. The mix contained a known amount of labeled phosphate in a total volume of 12 μl. After 5 min, 3 μl was spotted onto a nitrocellulose membrane and immediately washed with 5 ml of ice-cold BRB80 using a vacuum manifold (time between spotting and washing $\sim$2 sec). This was repeated twice in quick succession ($\sim$15 sec between membranes) for triplicate measurements in each condition. The amount of ^{32}P bound to each filter was determined by scintillation counting. The amounts of phosphate bound to filters from one such experiment are given in Table S2. Additional experiments were performed with incubation times of 5, 30, 60, and 180 min. All showed MCAK binding equal amounts of α- and γ- P_i while kinesin-1 did not retain the γ-P_i. This shows that kinesin-1 very rapidly hydrolyzes ATP and loses the terminal phosphate of ATP (ref. 27), while MCAK does not lose this phosphate. This indicates that kinesin-1 is predominantly in the ADP state in solution, while MCAK is in either the ATP or the ADP-P_i state. Furthermore, the results suggest that the functional difference between kinesin-1 and kinesin-13 family proteins is achieved through a major alteration in the hydrolysis mechanism.

Table S2 | Data for one ATP-phosphate binding experiment. Given are femtomoles of phosphate bound to each filter for the α- or γ- phosphate labeled ATP bound to MCAK (4 μM) and Kinesin-1 (0.2 μM) after 5 min incubation in radioactive ATPs (mean $\pm$ s.e.m., $n = 3$).

Phosphate	No protein	MCAK	Kinesin-1
[α -^{32} P]-ATP	244 $\pm$ 13	15758 $\pm$ 4714	965 $\pm$ 133
[γ -^{32} P]-ATP	463 $\pm$ 105	17903 $\pm$ 1141	226 $\pm$ 9

6 Detailed Methods

6.1 Protein expression details

For MCAK expression in insect cells the coding region of MCAK was PCR amplified from a human testis cDNA library and cloned into the pFastBac1 vector. PCR products including sequences coding His_6 and His_6-enhanced green fluorescent protein (eGFP) tags were amplified from pET_9alpha-His_6-eGFP and cloned 3' of MCAK gene. *Spodoptera frugiperda* (Sf9) cells expressed MCAK-His_6 and MCAK-His_6-eGFP after infection with virus generated using these plasmids (Invitrogen, BAC-TO-BAC expression system). Proteins were purified in a three-step process: cation exchange, metal-chelating, and desalting or gel filtration chromatography. Sf9 cells were dissolved in an equal volume of cold lysis buffer (50 mM HEPES pH 7.5, 150 mM NaCl, 5% glycerol, 0.1% Tween 20, 1.5 mM $MgCl_2$, 3 mM EGTA, 1 mM DTT, 0.5 mM Mg-ATP, protease inhibitors [1 mM phenylmethylsulfonyl fluoride, 10 μg/ml antipain, 5 μg/ml chymotrypsin, 20 μg/ml TPCK, 2 μg/ml aprotinin, 0.7 μg/ml pepstatin A, 0.5 μg/ml leupeptin, 20 μg/ml TAME, 1 mM benzamidine]). The crude lysate was clarified and loaded onto a SP-sepharose column (Amersham Biosciences HiTrap SP-HP). The column was washed with cation buffer (6.7 mM HEPES-/KOH pH 7.5, 6.7 mM MES, 6.7 mM sodium acetate, 150 mM NaCl, 1.5 mM $MgCl_2$, 10 μM Mg-ATP), and the protein was eluted from the column with a continuous salt gradient (150 mM-1 M NaCl) using a BioCAD SPRINT system. Peak fractions were pooled, brought to 9 mM imidazole, and loaded

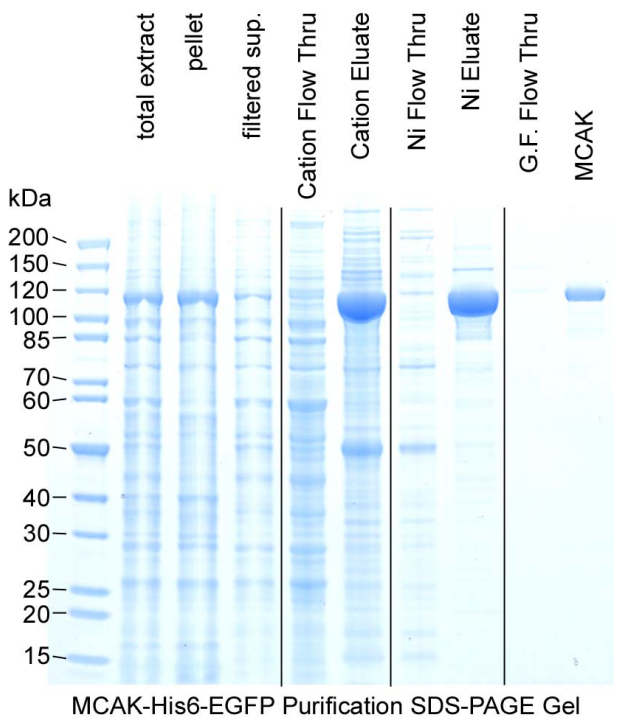

Figure S8 | SDS-PAGE Gel of MCAK-GFP Purification. MCAK-GFP appears as a 115 kDa band throughout the purification. The Ni column eluate is 90% pure, and the gel filtration column successfully removes the remaining contaminants (rightmost lane, labeled MCAK).

onto a Ni^{2+}-sepharose column (Amersham Biosciences HisTrap HP). The column was washed with imidazole buffer (50 mM $NaPO_4$ buffer pH 7.5, 300 mM NaCl, 9 mM imidazole, 10% glycerol, 1 mM $MgCl_2$, 10 μM Mg-ATP), and the protein was eluted with a continuous imidazole gradient (9 mM-180 mM). Peak MCAK-His_6 fractions were pooled and the buffer exchanged to storage buffer using a desalting column (Amersham Biosciences HiTrap Desalting). MCAK-His_6 was stored a $-80°C$ in 10% glycerol. In the case of MCAK-His_6-eGFP, peak Ni-column fractions were pooled and passed through a gel filtration column (Amersham Biosciences Superdex 200 16/60) pre-equilibrated with elution buffer, BRB80 (80 mM PIPES-/KOH pH 6.9, 1 mM $MgCl_2$, 1 mM EGTA) 150 mM KCl, 1 mM DTT and 10 μM Mg-ATP. Only the single peak fraction from the gel filtration column was used. Most experiments with MCAK-GFP were performed using freshly purified protein. Protein was stored with glycerol added to 10% in liquid N_2. Protein concentrations were estimated using a Bradford assay (Bio-Rad Protein Assay). Additionally, the concentration and the nucleotide state of active MCAK were determined using a filter-based ATP binding assay, using [α^{32}P]-ATP and [γ^{32}P]-ATP (ref. 30, see also Supplementary Information 5.2). Microtubule sedimentation assays (ref. 1) showed that both proteins depolymerized microtubules (data not shown).

6.2 Coverslip silanization

Microscope chambers were constructed using two silanized cover-slips separated by double-sided tape (Scotch 3M) such that channels 0.1 mm thick, 3 mm wide and 18 mm long are formed. Before silanization, 18 mm×18 mm and 22 mm×22 mm cover-slips (no. 1.5; Corning) were extensively cleaned by immersion in different solutions in the following order: 55 min in acetone, 10 min in ethanol, 1 min nano-pure water, 60 min in Pirnaha solution (H_2O_2/H_2SO_4, 3:5), three 1 min water rinses, 0.1 M KOH, and finally two 1 min water rinses before drying in nitrogen. Following 1-hour of silanization in 0.05% dichlorodimethylsilane in trichloroethylene, cover-slips were washed 4 times in methanol while sonicated. After 3 further rinses with nano-pure water, silanized cover-slips were stored dry. The coverslip/doublesided tape sandwich was assembled in cover-slip holders designed to allow imaging through the bottom cover-slip (22 mm×22 mm).

7 Legends for Supplementary movies

Movie 1 | MCAK induced microtubule depolymerization — Epifluorescence images (TRITC) of immobilized microtubules were recorded with 10 s intervals for 12 minutes. At 4 minutes, buffer containing 4 nM MCAK was added, resulting in the depolymerization of microtubules at 1.5 μm min^{-1}. Video playback is 100× real-time.

Movie 2 | MCAK diffusion in ATP — Immobilized microtubules (red) in buffer containing 1 mM ATP and 0.5 nM MCAK-GFP (green). The TIRF images (FITC) were recorded in continuous mode at 100 ms per frame and overlaid onto one static epifluorescence image (TRITC) of the microtubules. Video playback is in real-time.

Movie 3 | MCAK diffusion in ADP — Immobilized microtubules (red) in buffer containing 1 mM ADP and 0.5 nM MCAK-GFP (green). The TIRF images (FITC) were recorded in continuous mode at 100 ms per frame and overlaid onto one static epifluorescence image (TRITC) of the microtubules. Video playback is in real-time.

8 Additional References

S1. Berg, H. C. *Random walks in biology* (Princeton University Press, Princeton, N.J., 1993)